

Efficient anchor loss suppression in coupled near-field optomechanical resonators

Luiz, G. O., Santos, F. G. S., Benevides, R. S., Espinel, Y. A. V., Alegre, T. P. Mayer,
and Wiederhecker, G. S.^{a)}

*Gleb Wataghin Physics Institute, University of Campinas, 13083-859 Campinas,
SP, Brazil*

(Dated: June 9, 2022)

Elastic dissipation through radiation towards the substrate is a major loss channel in micro- and nanomechanical resonators. Engineering the coupling of these resonators with optical cavities further complicates and constrains the design of low-loss optomechanical devices. In this work we rely on the coherent cancellation of mechanical radiation to demonstrate material absorption and surface scattering limited silicon near-field optomechanical resonators oscillating at tens of MHz. The effectiveness of our dissipation suppression scheme is investigated at room and cryogenic temperatures. We demonstrate that the mechanical quality-factor temperature dependence is in good agreement with the Akhiezer effect down to 100 K. While at room temperature we can reach a maximum quality factor of 7.61k (Qf -product of the order of 10^{11} Hz), at 22 K the quality factor increases to 37k, resulting in a Qf -product of 2×10^{12} Hz.

^{a)}gustavo@ifi.unicamp.br

The interaction of optical and mechanical fields in microscale devices enables the manipulation and control of mechanical modes vibrating at radio-frequencies. Some remarkable examples resulting from such an optomechanical interaction include the preparation and measurement of harmonic oscillators' quantum ground states¹⁻³, optically induced synchronization between mechanical oscillators⁴, phase noise suppression⁵ and highly sensitive sensors^{6,7}. A major limitation in these microdevices is mechanical energy loss that leads to reduced sensitivity⁸, lower coherence⁹, and increased power consumption¹⁰, and remains among the most challenging issues in their design and fabrication processes.

While mechanical dissipation is ultimately limited by material absorption, it may also depend on the viscosity of the environment gas, anchor losses and surface scattering. Although the gas damping can be suppressed in vacuum, the necessary anchoring of micromechanical devices leads to radiation of mechanical waves towards the substrate, which is often the dominant dissipation channel. Fortunately, anchor dissipation can be reduced through phononic shielding^{11,12}, mesa isolation¹³, and destructive interference of elastic waves^{14,15}. Phononic shields are very effective for high frequency mechanical modes, but their large footprint¹⁶ at low frequencies can render them impractical. The mesa approach is efficient only for out-of-plane mechanical modes and its deep etch of the substrate may also be incompatible with photonic integration. On the other hand, exploring the destructive interference of mechanical waves is a simple method to obtain low frequency high- Q mechanical resonators, without impacting the device's design or footprint¹⁷. Although very low loss optical and mechanical devices have been reported^{16,18-20}, the constraints of simultaneously supporting optical and mechanical modes poses a challenge to optomechanical device's design. Near-field optomechanical (NFO) devices²¹⁻²³ can overcome that challenge as their mechanical and optical resonators are separated structures, which interact through the evanescent optical field.

Here we demonstrate a silicon NFO device that can reach material-limited quality factor by efficient suppression of anchor losses through elastic wave interference. Our NFO device is based on a mechanical resonator composed of coupled paddles that interact with a nearby silicon microdisk optical cavity (Fig. 1a). This design allows us to perfectly balance the mechanical waves radiated to the pedestal by each paddle without changes to the optical cavity design. Furthermore, our NFO paddle resonator design sets an interesting platform to study optomechanical arrays, as it allows coupling several mechanical resonators to a single optical cavity²⁴⁻²⁶.

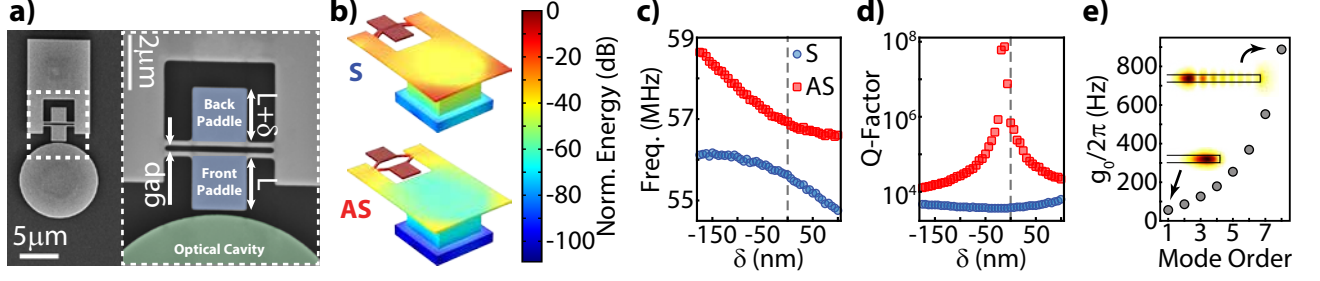


Figure 1. a) Scanning electron microscopy of the device; b) Finite element method (FEM) simulation of the normalized energy distribution of the mechanical modes of interest for the device with $\delta = -15$ nm in (c,d); c,d) Mechanical frequency and Q -factor dependence on paddles balance (δ) from FEM simulations; e) Perturbation theory estimate for the optomechanical coupling for different radial order optical TE modes with $\lambda = 1520$ nm; insets: $|E_r|$ distribution profiles of the first (bottom) and 8^{th} (top) radial order TE modes. In (b): Displacement is exaggerated and colors indicate normalized energy distribution. In (b-d) only radiation to the substrate is considered.

To obtain high- Q mechanical resonators we designed the double paddle NFO device shown in figure 1a. The mechanical resonator is composed by two square paddles ($2 \mu\text{m} \times 2 \mu\text{m}$), attached on both sides to suspended beams through 4 nanostrings (200 nm wide) separated by a 200 nm gap. The device is defined on a 200 nm silicon-on-insulator (SOI). Because the paddles' motion couple through the supporting beams, symmetric (S) and anti-symmetric (AS) combinations of individual paddle modes are formed, such as the in-plane modes shown in the finite element method (FEM) numerical simulation of Figure 1b. In order to reach a perfect balance between mechanical waves radiating to the supporting beams, the length of the back paddle (L) is offset from the front one by δ . FEM calculations of the mechanical modes show that the resonant frequencies of the coupled mechanical modes display the avoided crossing behavior when δ is varied (Fig. 1c), a signature of coupling between the paddles' motion. The calculations also show that the AS mode has consistently higher anchor loss limited Q 's when compared to the S mode (Fig. 1d). This difference appears because the S mode induces a larger displacement on the supporting beams, due to the two paddles' in-phase motion, coupling energy from the paddles to the pedestal and leading to a higher loss rate. On the other hand, the AS mode, due to the anti-phase paddle motion, drastically reduces the displacement at the anchor points, minimizing dissipation to the substrate when the two radiated mechanical waves are balanced. Moreover, we observe a

rapid increase of this effect when the paddles are more symmetric ($\delta \approx 0$), indicating that it is possible to eliminate anchor losses simply by balancing the paddles. Note however that the point of minimum dissipation of the AS mode happens with $\delta \approx -15$ nm, due to geometry asymmetry of the single-sided pedestal supporting the beams (Fig. 1a).

The devices were fabricated through the EpiXfab initiative at IMEC. They are defined on the 200 nm top silicon layer by deep UV photolithography and plasma etching at the foundry. The 2 μ m buried oxide is then partially removed using wet-etch (BOE) to define the pedestal and grant the device its mechanical degrees of freedom; this post-process step is performed in-house. Each die has a series of devices where the paddle farther from the disk (back paddle) has its length varied, while the other (front paddle) is fixed.

In order to readout the motion of the paddles, the front paddle is designed to be 200 nm away from a 5 μ m radius disk optical cavity (Fig. 1a) supporting whispering gallery modes²¹ (WGM). Optical readout is possible because the motion of the paddles modulates the frequencies of the WGM's through evanescent field perturbation. The figure of merit of this interaction is the optomechanical coupling rate, $g_0 = (\partial\omega/\partial x)x_{\text{zpf}}$, which measures the amount of optical frequency shift caused by the displacement amplitude of the quantum-mechanical zero-point fluctuation⁹ ($x_{\text{zpf}} = \sqrt{\hbar/4\pi m_{\text{eff}} f_m}$, where \hbar is the Planck's constant, m_{eff} the effective mass and f_m the resonance frequency). Although there are usually two main contributions to the optical resonance shift, namely boundary motion²⁷ and photo-elastic effect²⁸, we consider only moving boundary effects because the mechanical modes we are interested in induce negligible strain throughout the paddle volume. We employed perturbation theory²⁷ to calculate $\partial\omega/\partial x$ for the optical transverse electric (TE) modes, with various radial orders, due to the in-plane motion of the paddles and. Using FEM we determined the effective mass $m_{\text{eff}} \approx 3$ pg for both S and AS modes. The g_0 values ranging several hundred Hz, are shown in figure 1e.

To probe the devices we couple light from an external cavity tunable laser into the disk resonator through a tapered fiber (Fig. 2a). The transmitted signal reveals the microdisk optical resonances (Fig. 2b), which usually exhibit frequency splitting due to counter-propagating optical mode coupling, induced by surface roughness and paddle-induced scattering (Fig. 2c). Nevertheless, these modes present high loaded optical quality factors of about $Q_{\text{opt}} = 40\text{k}$. The optical mode used to probe the mechanical motion is chosen by monitoring the radio-frequency power spectrum strength at the resonant mechanical frequency, which depends on

g_0 , optical linewidth (κ), and taper-cavity loading conditions²⁹. Although we cannot identify exactly which optical mode (radial and azimuthal order) is excited, comparison of the measured optical free spectral range (FSR) with FEM simulations over a broad range (1460 nm to 1610 nm — not shown), indicates that we are coupling to higher radial order TE modes; indeed, good agreement between experimental and theoretical values for g_0 also supports this assumption (Fig. 1e). Measurement of g_0 and calibration of the PSD into a displacement noise spectrum density [$\text{m}/\text{Hz}^{1/2}$] is performed using a calibrated phase-modulation tone close to the mechanical resonances²⁹. The mechanical modes are identified by directly comparing measured frequencies with those from FEM simulations, which agree within a 2% margin. All measurements are performed with the optical cavity undercoupled to the taper.

The room temperature (RT) mechanical quality factors (Q_m) are obtained from the measured power spectral density (PSD) of the two in-plane mechanical modes while the sample is in a vacuum chamber (10^{-5} mbar). Using an homodyne detection scheme³⁰ we are able to probe the samples with the laser tuned to the center of the optical resonance, thus avoiding any optomechanical feedback that could affect the mechanical quality factor. In Figure 3(a,b) (orange curves) we show the measured PSD's and their fitted Lorentzians for the device with $\delta = -50$ nm, which has the highest AS mode quality factor, $Q_{m,\text{AS}}^{\text{RT}} = (7.61 \pm 0.07)\text{k}$, and the S mode quality factor $Q_{m,\text{S}}^{\text{RT}} = (4.53 \pm 0.04)\text{k}$. The mechanical resonance frequencies of these coupled modes are around $f_m = 56$ MHz with a frequency splitting of $\Delta f_m = 940$ kHz, also in good agreement with the FEM simulations; this corresponds to a Qf -product of 4×10^{11} Hz. A confirmation that the $\delta = -50$ nm device is the one with best anchor loss suppression can be drawn from the frequency and optomechanical couplings measured for devices with varying balance between paddles, as shown in figures 3(c,d). This device not only has the smallest frequency difference but it also has S/AS modes with almost identical measured optomechanical coupling rates ($g_0 \approx 2\pi 450$ Hz). Since g_0 is a direct indicator of the motional amplitude of the front paddle in each mode, the data in figure 3d also suggest that this paddle motion has the same amplitude for both modes. We note that the experimental best balance of mechanical waves radiation occurs for a δ different from that of simulations. This might be explained by deviations in the devices geometries, such as the rounded corners in the clamping regions of the nanostrings.

Comparison of the S and AS modes' quality factors, for devices with different δ (Fig. 3e),

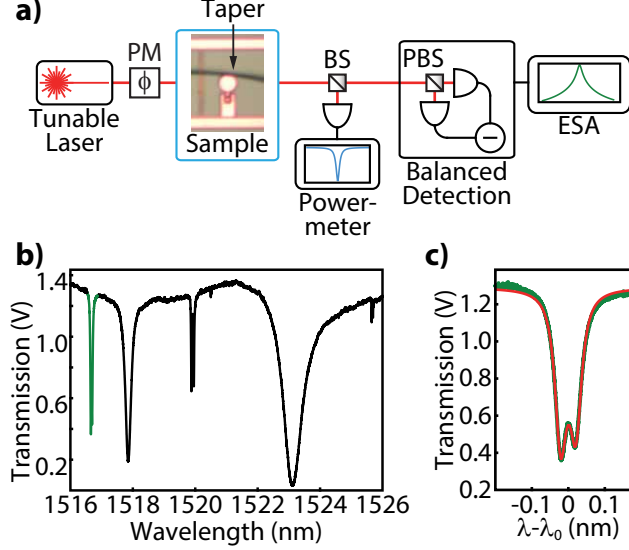


Figure 2. a) Schematics of the experimental setup; b) Broad optical spectrum of a typical device - marked in green is the resonance used to probe the mechanical modes; c) Measured resonance (green) and fitted counter-propagating coupled modes function (red) - $\lambda_0 = 1516.68$ nm and loaded quality factor $Q_{opt} = 40k$. In (a): PM = phase-modulator; BS = beam splitter; PBS = polarizing beam splitter; ESA = electric spectrum analyzer. In (c): fitted peak is the same marked in (b).

shows consistently higher quality factors for the AS modes, suggesting an important contribution from anchor loss. Nevertheless, its modest two-fold improvement compared to the S mode — even for the best resonator — indicates that other loss mechanisms are also playing an important role in the overall dissipation. To suppress temperature dependent mechanisms and intensify the role of our radiation suppression scheme in the overall mechanical losses, we insert the sample in a cold-finger cryostat to cool the sample down to 22 K. At these low temperatures (LT), we observe a high enhancement of 385% for the AS mode quality factor, reaching $Q_{m,AS}^{LT} = (37.0 \pm 0.6)k$ (Fig. 3b, green curve), while the S mode increases only by 80%, up to $Q_{m,S}^{LT} = (8.2 \pm 0.1)k$ (Fig. 3a, green curve), for the better balanced device. These Q -enhancements are accompanied by a small (0.7%) increase in mechanical frequencies due to an expected material stiffening at LT, resulting in a Qf -product of 2×10^{12} Hz. Such a high contrast between the S/AS modes' quality factors at LT clearly indicates the efficiency of the destructive interference scheme. Also, the LT limit for the Q_m of the S mode is in good quantitative agreement with the FEM simulations (Fig. 1d). Nonetheless, the calculated anchor loss limited Q_m is much higher for the AS mode, around 10^8 , an indication

that we may have reached some kind of material limit at 22 K.

We investigate the nature of the low temperature Q -limit by increasing the cryostat base temperature from 22 K up to 200 K, while monitoring the mechanical quality factors (Fig. 3g). The measured Q temperature dependence reveals a capped behavior below ~ 100 K and a power-law reduction above. We interpret the power-law dependence above 100 K as a material-dependent mechanism. Two common material related loss channels in silicon devices are the thermoelastic damping (TED)³¹, caused by heat flow between mechanically heated regions, and the Akhiezer damping (AKD)^{32,33}, in which the strain locally distort the mechanical waves dispersion, driving thermal phonons out of equilibrium and restoring it through dissipative scattering. We use FEM calculations (Fig. 3h) to determine the expected room-temperature TED-limited Q 's for our devices to be around 10^5 , well above the measured values. Moreover, because TED is proportional to the thermal expansion coefficient — which decreases at low temperature for silicon — the low temperature TED-limited Q 's are at the 10^6 level, hence TED does not explain neither the LT nor the temperature dependent and RT Q_m limits.

To assess the role of the Akhiezer effect we fit to our data the analytical model for this effect³³ (Fig. 3g, solid lines), plus a constant contribution to account for the plateau below 100 K: $Q_{m,\text{tot}} = (2\pi f_m)/(\Gamma_p + \eta\Gamma_{\text{AKD}})$, with free parameters Γ_p , for the plateau, and η . The mechanical frequency, f_m , is fixed at the measured values and Γ_{AKD} is the temperature-dependent AKD damping rate, $\Gamma_{\text{AKD}} = 4\pi^2\gamma^2 f_m^2 c_v \tau T / 3\rho V^2$, which depends on temperature (T) not only directly but also through material properties, such as the Grüneisen parameter³⁴ (γ), specific heat³⁵ (c_v), thermal phonon relaxation time³⁶ (τ) and sound velocity³⁶ (V). With the exception of density (ρ), which has a negligible variation over the measured temperature range, we included the published temperature dependencies of all parameters. The Grüneisen parameter is the one with the largest range of reported values^{37,38} and, to account for this, we used the temperature dependence reported by Philip and Breazeale³⁴, but included in our model an overall scaling parameter η . As a result we obtained a very good agreement on the power-law above 100 K, with a fitted $\eta = 17.7$. Despite its large value, if the scaling parameter η is absorbed into the Grüneisen parameter, it would correspond to a room-temperature parameter $\gamma \rightarrow \gamma\sqrt{\eta} = 1.9$, which is only 25% larger than the more common $\gamma \approx 1.5$ used for bulk samples³⁷. Nevertheless, this is a good indication that our devices are AKD-limited for temperatures above 100 K.

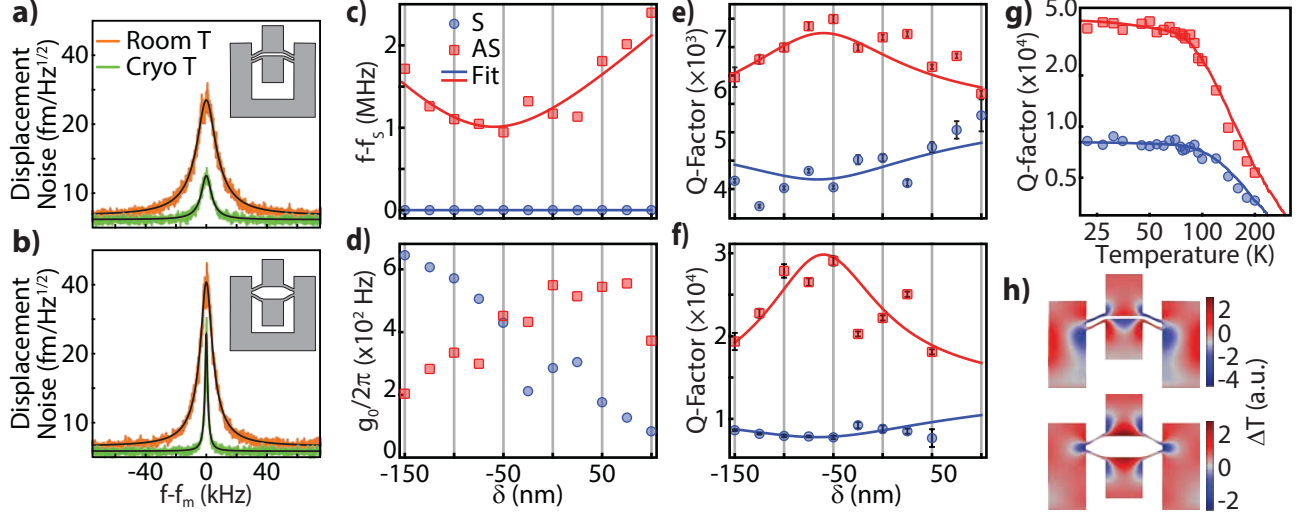


Figure 3. a,b) S (a) and AS (b) modes calibrated power spectrum density at room (orange) and cryogenic (green) temperatures; c-f) Asymmetry dependence of frequency difference between S (blue) and AS (red) modes at room temperature (c), g_0 calibrated at room temperature (d), Q -factor at room (e) and cryogenic (f) temperatures; g) Temperature dependence of quality factor in $\log \times \log$ scale; h) Top view of 3D FEM simulation of thermoelastic effect temperature variation, which leads to TED limited Q 's close to 100k at room temperature. In a,b): colored lines are data while black are fitted Lorentzians. In c-g): marks represent experimental data and solid lines are fitted curves (see text). In (g) all points were measured with device out of thermal equilibrium. In a,b,g): device with $\delta = -50$ nm.

The capping behavior observed below 100 K, which is not explained either by AKD or TED, could be attributed to a residual asymmetry in our fabricated paddles. To investigate this possibility we fitted a three coupled mass-spring lumped oscillators model¹⁵ to the room-temperature resonance frequency curves ($f - f_s$) shown in Fig. 3c. The low-temperature frequency data is not shown, but matches the data in Fig. 3c within 0.7%. The same analytical model also fits well to the quality factor data for both RT (Fig. 3e) and LT (Fig. 3f). Both data and model confirm that the S mode is limited by anchor losses, specially at 22 K (Fig. 3f), in quantitative agreement with the FEM simulations. On the other hand, the slowly varying AS mode Q -enhancement, towards the higher symmetry region ($\delta \approx 0$), suggests that the Q is not being limited by variations in the device geometry. We also verified through numerical simulations that small (± 100 nm) variations on any of the device transverse dimensions would not quench the AS quality factors to the LT measured

levels. Hence, we infer that the AS mode LT Q -factor is not being limited by failure of the destructive interference scheme, but instead by some surface-related dissipation. One experimental evidence that this upper Q -limit is related to surface effects is the variation of the quality factors at successive cool downs of our sample. Noticeably, the data in Fig. 3f was taken in a second cool down of the same die used for Fig. 3(a,b) measurements, and it already shows a maximum $Q_{m,AS}^{LT} = 28k$ that is 24% smaller than the first cool down value (the sample was kept in low vacuum, approximately 10^{-2} mbar, between cool downs). This observation agrees with previous reports of surface dissipation^{39–42} in thin silicon devices, where the high surface area to volume ratio may lead to severe divergence from standard bulk dissipation.

In summary, we have demonstrated the use of destructive interference of elastic waves as an effective approach to obtain high- Q mechanical resonators. Our data clearly shows that symmetric modes are highly susceptible to anchor loss, while the antisymmetric modes may be limited by other absorption mechanisms, such as the Akhiezer effect and surface scattering. To further increase these devices' performance one should pay attention to the fabrication process as well as storage conditions, reducing surface related dissipation and increasing the low temperature Q limit for the AS mode. To overcome the limitation posed by AKD at room temperature one must look for higher frequency modes/devices or different materials. We expect these devices to serve as platforms for studies of arrays of optically coupled mechanical resonators, as well as very sensitive force sensors.

This work was supported with funds from FAPESP (grants: 2008/57857-2, 2012/17610-3, 2012/17765-7) and CNPq (grant 153044/2013-6).

REFERENCES

- ¹J. Chan, T. P. M. Alegre, A. H. Safavi-Naeini, J. T. Hill, A. Krause, S. Gröblacher, M. Aspelmeyer, and O. Painter, *Nature* **478**, 89 (2011).
- ²L. Ying, Y.-C. Lai, and C. Grebogi, *Physical Review A* **90**, 053810 (2014).
- ³M. Ludwig and F. Marquardt, *Physical Review Letters* **111**, 073603 (2013).
- ⁴M. Zhang, G. S. Wiederhecker, S. Manipatruni, A. Barnard, P. McEuen, and M. Lipson, *Physical Review Letters* **109**, 233906 (2012), arXiv:1112.3636.
- ⁵M. Zhang, S. Shah, J. Cardenas, and M. Lipson, *Physical Review Letters* **115**, 163902

- (2015), arXiv:1505.02009.
- ⁶F. Liu, S. Alaie, Z. C. Leseman, and M. Hossein-Zadeh, Optics express **21**, 19555 (2013).
- ⁷F. Guzmán Cervantes, L. Kumanchik, J. Pratt, and J. M. Taylor, Applied Physics Letters **104**, 221111 (2014), arXiv:1303.1188.
- ⁸C. Huang, J. Fan, R. Zhang, and L. Zhu, Optics Express **21**, 6371 (2013), arXiv:1303.0440.
- ⁹M. Aspelmeyer, T. J. Kippenberg, and F. Marquardt, Reviews of Modern Physics **86**, 1391 (2014).
- ¹⁰T. Kippenberg, H. Rokhsari, T. Carmon, A. Scherer, and K. Vahala, Physical Review Letters **95**, 033901 (2005).
- ¹¹T. Alegre and A. Safavi-Naeini, Optics Express **19**, 5658 (2010).
- ¹²F.-C. Hsu, J.-C. Hsu, T.-C. Huang, C.-H. Wang, and P. Chang, Journal of Physics D: Applied Physics **44**, 375101 (2011).
- ¹³M. Pandey, R. Reichenbach, A. Zehnder, A. Lal, and H. Craighead, Journal of Microelectromechanical Systems **18**, 836 (2009).
- ¹⁴S. A. Zotov, B. R. Simon, I. P. Prikhodko, A. A. Trusov, and A. M. Shkel, IEEE Sensors Journal **14**, 2706 (2014).
- ¹⁵M. Zhang, G. Luiz, S. Shah, G. Wiederhecker, and M. Lipson, Applied Physics Letters **105**, 051904 (2014), arXiv:1406.0029.
- ¹⁶Y. Tsaturyan, A. Barg, E. S. Polzik, and A. Schliesser, (2016), arXiv:1608.00937.
- ¹⁷R. Zhang, C. Ti, M. I. Davanço, Y. Ren, V. Aksyuk, Y. Liu, and K. Srinivasan, Applied Physics Letters **107**, 131110 (2015), arXiv:1508.00067.
- ¹⁸D. K. Armani, T. J. Kippenberg, S. M. Spillane, and K. J. Vahala, Nature **421**, 925 (2003).
- ¹⁹S. S. Verbridge, J. M. Parpia, R. B. Reichenbach, L. M. Bellan, and H. G. Craighead, Journal of Applied Physics **99**, 124304 (2006).
- ²⁰R. Norte, J. Moura, and S. Gröblacher, Physical Review Letters **116**, 147202 (2016).
- ²¹G. Anetsberger, O. Arcizet, Q. P. Unterreithmeier, R. Rivière, A. Schliesser, E. M. Weig, J. P. Kotthaus, and T. J. Kippenberg, Nature Physics **5**, 909 (2009).
- ²²K. Srinivasan, H. Miao, M. T. Rakher, M. Davanço, and V. Aksyuk, Nano letters **11**, 791 (2011).
- ²³P. H. Kim, C. Doolin, B. D. Hauer, A. J. R. MacDonald, M. R. Freeman, P. E. Barclay, and J. P. Davis, Applied Physics Letters **102**, 053102 (2013), arXiv:1210.1852v2.

- ²⁴A. Xuereb, C. Genes, and A. Dantan, Physical Review Letters **109**, 223601 (2012), arXiv:1202.6210.
- ²⁵A. Xuereb, C. Genes, G. Pupillo, M. Paternostro, and A. Dantan, Physical Review Letters **112**, 133604 (2014).
- ²⁶C. A. Holmes, C. P. Meaney, and G. J. Milburn, Physical Review E **85**, 066203 (2012), arXiv:1105.2086.
- ²⁷S. G. Johnson, M. Ibanescu, M. A. Skorobogatiy, O. Weisberg, J. D. Joannopoulos, and Y. Fink, Physical Review E **65**, 066611 (2002).
- ²⁸J. Chan, A. H. Safavi-Naeini, J. T. Hill, S. Meenehan, and O. Painter, Applied Physics Letters **101**, 081115 (2012).
- ²⁹M. L. Gorodetsky, A. Schliesser, G. Anetsberger, S. Deleglise, and T. J. Kippenberg, Optics Express **18**, 23236 (2010), arXiv:1009.4231.
- ³⁰T. Hansch and B. Couillaud, Optics Communications **35**, 441 (1980).
- ³¹R. Lifshitz and M. L. Roukes, Physical Review B **61**, 5600 (2000).
- ³²A. Akhiezer, Journal of Physics-USSR **1**, 277 (1939).
- ³³T. O. Woodruff and H. Ehrenreich, Physical Review **123**, 1553 (1961).
- ³⁴J. Philip and M. A. Breazeale, Journal of Applied Physics **54**, 752 (1983).
- ³⁵P. D. Desai, Journal of Physical and Chemical Reference Data **15**, 967 (1986).
- ³⁶S. D. Lambade, G. G. Sahasrabudhe, and S. Rajagopalan, Physical Review B **51**, 15861 (1995).
- ³⁷S. Ghaffari, S. A. Chandorkar, S. Wang, E. J. Ng, C. H. Ahn, V. Hong, Y. Yang, and T. W. Kenny, Scientific Reports **3**, 3244 (2013).
- ³⁸D. S. Kim, H. L. Smith, J. L. Niedziela, C. W. Li, D. L. Abernathy, and B. Fultz, Physical Review B **91**, 014307 (2015).
- ³⁹R. Mihailovich and N. MacDonald, Sensors and Actuators A: Physical **50**, 199 (1995).
- ⁴⁰J. Yang, T. Ono, and M. Esashi, Applied Physics Letters **77**, 3860 (2000).
- ⁴¹J. A. Henry, Y. Wang, and M. A. Hines, Applied Physics Letters **84**, 1765 (2004).
- ⁴²S. Reid, G. Cagnoli, D. Crooks, J. Hough, P. Murray, S. Rowan, M. Fejer, R. Route, and S. Zappe, Physics Letters A **351**, 205 (2006).